Nano Research 2018, 11(11): 6102–6109
https://doi.org/10.1007/s12274-018-2128-3
Research Article
ISSN 1998-0124
CN 11-5974/O4

Bandgap broadening at grain boundaries in single-layer MoS_2

Dongfei Wang[1,§], Hua Yu[1,§], Lei Tao[1,§], Wende Xiao[2] (✉), Peng Fan[1], Tingting Zhang[1], Mengzhou Liao[1], Wei Guo[2], Dongxia Shi[1], Shixuan Du[1] (✉), Guangyu Zhang[1] (✉), and Hongjun Gao[1]

[1] *Institute of Physics & University of Chinese Academy of Sciences, Chinese Academy of Sciences, Beijing 100190, China*
[2] *School of Physics, Beijing Institute of Technology, Beijing 100081, China*
[§] *Dongfei Wang, Hua Yu, and Lei Tao contributed equally to this work.*

Received: 16 December 2017
Revised: 23 April 2018
Accepted: 14 June 2018

KEYWORDS
MoS_2,
grain boundary,
bandgap,
scanning tunneling microscopy

ABSTRACT

Two-dimensional semiconducting transition-metal dichalcogenides have attracted considerable interest owing to their unique physical properties and future device applications. In particular, grain boundaries (GBs) have been often observed in single-layer MoS_2 grown via chemical vapor deposition, which can significantly influence the material properties. In this study, we examined the electronic structures of various GBs in single-layer MoS_2 grown on highly oriented pyrolytic graphite using low-temperature scanning tunneling microscopy/spectroscopy. By measuring the local density of states of a series of GBs with tilt angles ranging from 0° to 25°, we found that the bandgaps at the GBs can be either broadened or narrowed with respect to the intrinsic single-layer MoS_2. The bandgap broadening shows that the GBs can become more insulating, which may directly influence the transport properties of nanodevices based on polycrystalline single-layer MoS_2 and be useful for optoelectronics.

1 Introduction

Since the discovery of graphene in 2004 [1], the epitaxial growth and electronic structure of two-dimensional (2D) transition-metal dichalcogenides—particularly single-layer molybdenum disulfide (MoS_2) with a direct bandgap of ~ 2.4 eV [2]—on various substrates have attracted tremendous interest [3–7]. This structure offers a platform for investigating many new concepts in physics, such as the valley Hall effect [8], spin-valley locking [9], and the metal–insulator transition [10] and so on [11–13]. However, grain boundaries (GBs), which are one-dimensional line defects that mediate the transition from one crystalline orientation to another, are often observed in single-layer MoS_2 grown via chemical vapor deposition (CVD) [14–18]. As the atomic arrangements at the GBs differ significantly from the perfect lattice of single-layer MoS_2, the local electronic

Address correspondence to Wende Xiao, wdxiao@bit.edu.cn; Shixuan Du, sxdu@iphy.ac.cn; Guangyu Zhang, gyzhang@iphy.ac.cn

structures around the GBs can be greatly altered with respect to that of perfect single-layer MoS_2. Thus, the macroscopic properties, e.g., the optoelectronic and transport properties, of CVD-grown single-layer MoS_2 can deviate significantly from those of perfect single-layer MoS_2. Therefore, it is of great importance to clarify the structural and electronic properties of the GBs in such CVD-grown single-layer MoS_2.

In recent years, many efforts have been made to understand the physical properties of the GBs in 2D MoS_2 [19–24]. The atomic structures of the GBs in 2D MoS_2 have been intensively studied via transmission electron microscopy, and a variety of dislocation cores, such as 4|4, 5|7, 6|8, and 4|6 structures, have been revealed [14, 15, 25]. These tilted GBs were found to impose a significant degradation effect on the mobility and transport characteristics of MoS_2 [20]. The tilted GBs in single-layer MoS_2 were predicted to exhibit gap states, according to density functional theory (DFT) calculations [19]. It was shown that GBs with a tilt angle of 60° can exhibit a metallic feature [19], similar to the metallic GBs in single-layer graphene [26, 27]. Recently, Huang et al. investigated the electronic structures of GBs with various tilt angles in CVD-grown single-layer MoS_2 via scanning tunneling microscopy/spectroscopy (STM/STS) and observed a significant bandgap reduction for all GBs due to the combination of local strain fields and substrate-induced charge transfer [21]. It is well known that the bandgap of a semiconductor can be either narrowed or broadened by applying different strain. However, bandgap broadening has not been reported for the GBs in single-layer MoS_2 to date, even though abundant GBs with different tilt angles—and therefore with variable strain—are formed in practical CVD-grown single-layer MoS_2.

In this study, we investigate the bandgap broadening at the GBs in single-layer MoS_2 grown on highly oriented pyrolytic graphite (HOPG) via low-temperature (LT) STM/STS. By measuring the local density of states (DOS) of a series of GBs with tilt angles ranging from 0° to 25°, we find that the bandgaps at the GBs can be either broadened or narrowed with respect to the intrinsic single-layer MoS_2. The bandgap broadening shows that the GBs can become more insulating, which may directly influence the transport properties of nanodevices based on polycrystalline single-layer MoS_2 and be useful for optoelectronics.

2 Results and discussion

Single-layer MoS_2 was grown on HOPG via CVD to obtain various GBs. Because the step edges of HOPG serve as a nucleation center for the growth of single-layer MoS_2 and the orientations of the nuclei are random, GBs with various tilt angles can be formed [7], as schematically illustrated in Fig. 1(a). Atomic force microscopy (AFM) measurements confirm that the MoS_2 grows along the step edge of HOPG, as shown in Fig. 1(b). Figure 1(c) displays a typical STM image of the as-grown MoS_2. Line profile analysis reveals an apparent height of ~ 8 Å (Fig. 1(c)) with respect to the HOPG substrate, showing that the as-grown MoS_2 is single-layer, in agreement with a previous report [21]. The two linear protrusions (indicated by the white arrows) in the MoS_2 island shown in Fig. 1(c) are assigned to GBs [21]. High-resolution STM images, as presented in Fig. 1(d), disclose a hexagonal lattice of the top-layer sulfur atoms of MoS_2 and the moiré patterns originating from the lattice mismatch and misalignment of the MoS_2 and substrate [28, 29]. Figure 1(e) shows a representative differential conductance (dI/dV) spectrum (average over 100 spectra) collected in the perfect MoS_2 regions without any defects. A bandgap of ~ 2.7 eV is measured for the single-layer MoS_2 grown on HOPG, coincident with previous experiments and theoretical calculations [21, 30, 31]. Figure 1(f) illustrates the Raman spectrum of the single-layer MoS_2 grown on HOPG. Both the line shape and the peak positions are in accordance with previous reports [32].

Figure 2 shows a selected set of GBs with different tilt angles in the single-layer MoS_2 grown on HOPG. The tilt angles are directly derived from the atomic-resolution STM images of the neighboring MoS_2 domains. The MoS_2 domains around the GBs exhibit different moiré patterns, owing to the different twisting angles between the lattices of the MoS_2 and substrate [29]. The STM topographies of the GBs are more sensitive to the sample bias than those of the neighboring MoS_2 domains (see Fig. 2(d) and Figs. S1(a), S1(c)–S1(f) in the Electronic Supplementary Material

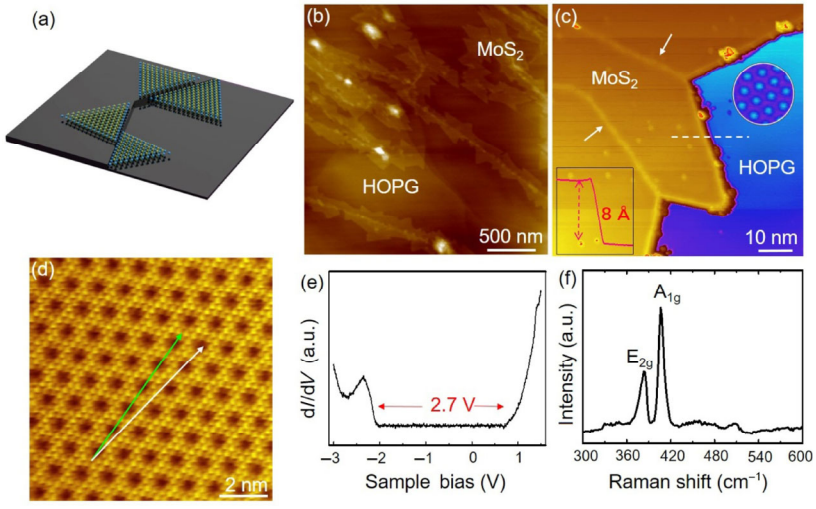

Figure 1 Characterization of MoS_2 grown on the HOPG substrate. (a) Cartoon illustrating the growth of single-layer MoS_2 triangle islands along the step edges of HOPG. (b) Large-scale AFM image showing the formation of GBs between the MoS_2 islands. (c) STM image of the as-grown single-layer MoS_2 with two GBs (indicated by the two white arrows). The bottom-left inset shows the line profile along the white dashed line. The top-right inset shows the atomic resolution of the HOPG substrate. Sample bias: $U = -3.97$ V; set point: $I = 30$ pA. (d) High-resolution STM image showing the hexagonal lattice of the top-layer sulfur atoms of MoS_2 and the moiré patterns. The green and white arrows are along the lattice vectors of the Moiré pattern and MoS_2, respectively. $U = -1.48$ V; $I = 10$ pA. (e) Averaged dI/dV spectrum obtained on a perfect MoS_2 surface showing a bandgap of ~ 2.7 eV. (f) Raman spectrum of the as-grown single-layer MoS_2 on HOPG.

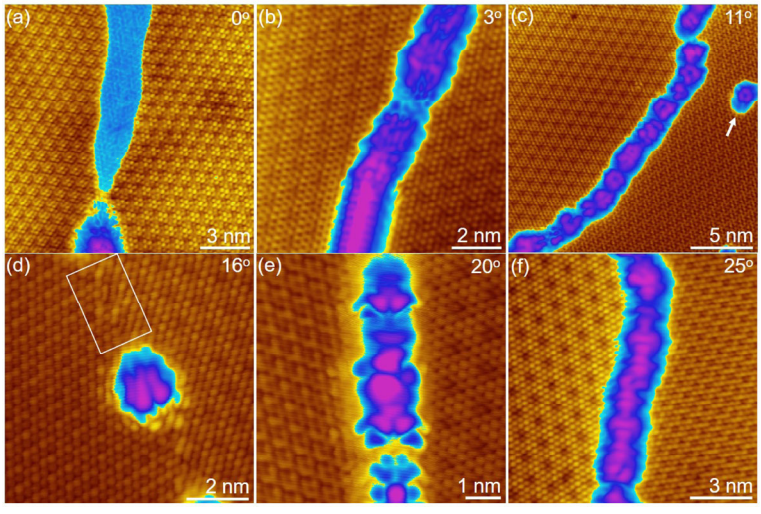

Figure 2 High-resolution STM images of six MoS_2 GBs with different tilt angles (θ). (a) $\theta = 0°$, $U = -2.0$ V, $I = 12$ pA; (b) $\theta = 3°$, $U = -0.5$ V, $I = 12$ pA; (c) $\theta = 11°$, $U = -1.1$ V, $I = 55$ pA. The white arrow indicates a point defect showing a scattering pattern with threefold symmetry. (d) $\theta = 16°$, $U = -0.5$ V, $I = 40$ pA. The region marked by the white rectangle exhibits significant lattice mismatch and distortion around the GB. (e) $\theta = 20°$, $U = -0.9$ V, $I = 81$ pA. (f) $\theta = 25°$, $U = -0.7$ V, $I = 102$ pA.

(ESM)), suggesting different electronic structures of the GBs relative to their neighboring MoS_2 domains. It is well known that the defects, including point defects, GBs, and step edges, can effectively scatter the electrons, forming certain scattering patterns that strongly depend on the detailed atomic structures of the defects [33, 34]. For instance, a threefold symmetric scattering pattern is formed around the point defect depicted in Fig. 2(c). For the GBs consisting of various dislocations, such as 5|7 and 6|8 structures [15, 19], the scattering patterns around them are usually rather complicated, hindering the straightforward

distinguishing of the atomic structures of the GBs. Figure 2(d) illustrates a butterfly-shaped scattering pattern, which most likely corresponds to a dislocation core, similar to that in single-layer WSe_2 grown on graphite [35]. Significant distortion is clearly observed in the region (marked by the white rectangle in Fig. 2(d)) along the GB and close to the dislocation core. Such lattice distortion may result in considerable strain in the MoS_2 lattice and thus modification of the topographies and electronic structures around the GBs. Notably, the GBs always show wrinkle structures in STM topographies (see Figs. 2, 3(a), and 3(e) and Table S1 in the ESM), indicating the presence of a vertical strain perpendicular to the plane of the MoS_2 lattice, in addition to lateral strains. Thus, the strain built up around the GBs is biaxial and highly spatially dependent.

To explore the electronic structures of the GBs in detail, we systematically collected a series of dI/dV spectra along and across a family of GBs with different tilt angles. Figure 3 displays two sets of representative data. The GB with a tilt angle of 16° shown in Fig. 3(a) (see Fig. 2(d) and Fig. S1(a) in the ESM) consists of a nearly ordered row of dislocation cores with butterfly-shaped scattering patterns. The dI/dV spectra (Fig. 3(b)) acquired across this GB show that the valence-band maximum (VBM) is nearly pinned at −2 eV, while the conductance-band minimum (CBM) is shifted from 0.8 eV for the intrinsic single-layer MoS_2 to 2.4 eV for the GB (see Fig. 3(c)). The bandgap increases with the decreasing distance to the GB, as shown in Fig. 3(c). An unprecedented bandgap of 4.4 eV is measured at the GB, which is far larger than that of 2.7 eV for the intrinsic single-layer MoS_2 far from the GB. This type of GB behaves as an insulator, possibly having a significant impact on the transport properties of the epitaxial single-layer MoS_2. The dI/dV spectra (Fig. 3(d)) acquired along this GB show that the bandgap varies at different sites of the GB. The bandgap at the center of a dislocation core is narrower than that between two neighboring dislocation cores. This spatially dependent behavior of the bandgap straightforwardly

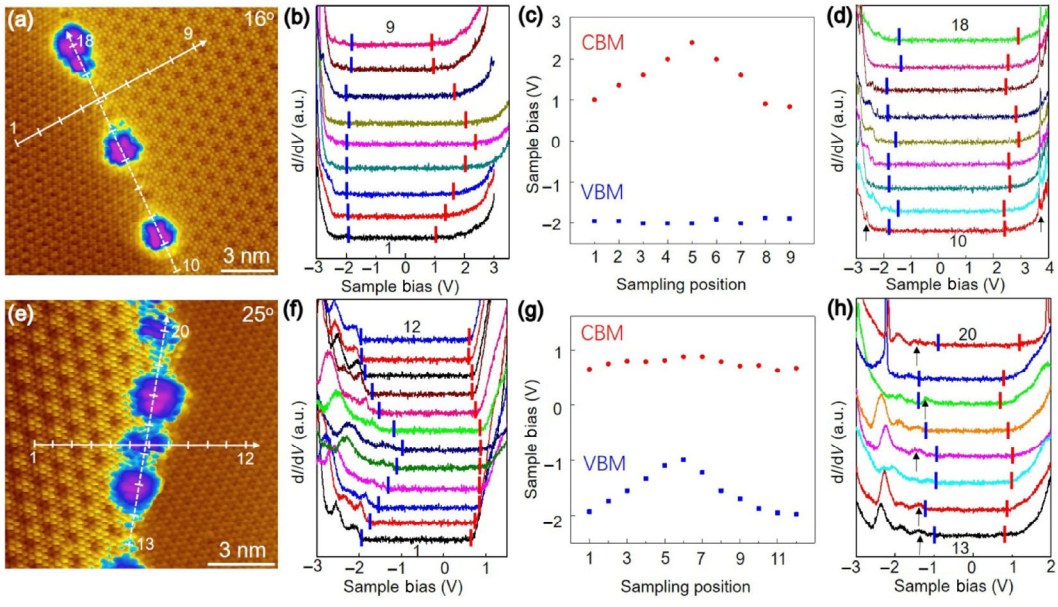

Figure 3 Bandgap variation on and around two representative GBs. (a) STM image of a GB with a tilt angle of 16° showing a nearly ordered array of butterfly-shaped scattering patterns. U = −0.5 V, I = 11 pA. (b) and (d) dI/dV spectra collected across (arrow with points 1–9) and along (arrow with points 10–18) the GB shown in (a), respectively. The CBM and VBM are indicated by the red and blue vertical lines. The two peaks indicated by the black arrows in each spectrum are assigned to von Hove singularities. (c) CBM and VBM energy diagram determined from the dI/dV spectra collected across (points 1–9) the GB shown in (b). (e) STM image of a GB with a tilt angle of 25°. U = −0.21 V; I = 152 pA. (f) and (h) dI/dV spectra acquired across (arrow with points 1–12) and along (arrow with points 13–20) the GB shown in (e), respectively. The CBM and VBM are indicated by the red and blue vertical lines, respectively. The features indicated by the black arrows are attributed to the defect states. (g) CBM and VBM energy diagram determined from the dI/dV spectra collected across (points 1–12) the GB shown in (f).

demonstrates that the electronic structures of the GBs are essentially determined by their local atomic structures. Notably, each spectrum in Fig. 3(d) exhibits two sharp peaks (indicated by the black arrows) near the VBM and CBM. As this GB consists of a nearly ordered row of dislocation cores, we attribute these sharp peaks to von Hove singularities, similar to the case of GBs in single-layer graphene [36, 37].

Figure 3(e) shows a GB with a tilt angle of ~ 25°. This GB also consists of a row of dislocation cores but with some disorder. The dI/dV spectra collected across this GB are plotted in Fig. 3(f). The bandgap decreases with the decreasing distance to the GB and reaches a minimum of ~ 2 eV at the GB, indicating that this GB exhibits more metallic behavior than the intrinsic single-layer MoS_2. In addition, both the CBM and VBM shift upwards with the decreasing distance to the GB (see Fig. 3(g)). The dI/dV spectra acquired along this GB (Fig. 3(h)) also show a spatially dependent behavior of the bandgap, again indicating that the electronic structures of the GBs are essentially determined by their local atomic structures. We observe additional peaks in the dI/dV spectra acquired at different sites of the GB, as indicated by the black arrows in Fig. 3(h). These peaks are located approximately −1.4 eV below the Fermi level and are localized at the dislocation core. The emergence of these localized states leads to significant deformation of the valence band edge and thus a reduced bandgap at the GB. These behaviors are very similar to a recent report of GBs in single-layer WSe_2 [35]. Moreover, the tensile strain observed at the vicinity of the GBs can lead to the reduction of the bandgap, akin to previous works by Huang et al. [21].

We measured the bandgaps of 11 GBs with tilt angles ranging from 0° to 25°. Figure 4(a) presents the statistical analysis of our measurements as well as the results of Huang et al. [21]. It is clearly observed that approximately half of the GBs exhibit a broadened bandgap with respect to the intrinsic single-layer MoS_2, while the other half show a narrowed one. This is different from previous experimental observations and theoretical predictions that the GBs of MoS_2 always show a narrowed bandgap [19].

As the bandgap narrowing at the GBs in single-layer MoS_2 was previously reported and the underlying

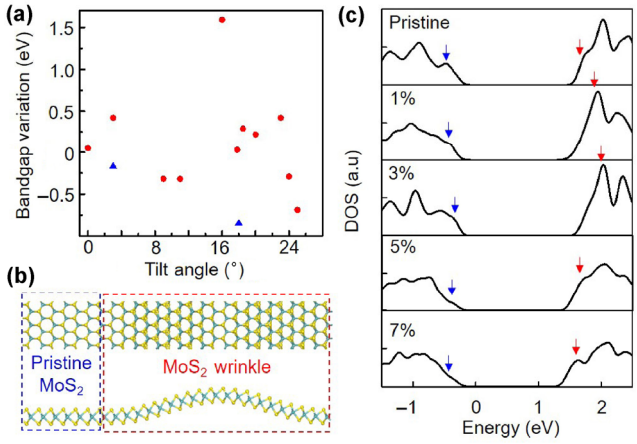

Figure 4 Theoretical model for the bandgap broadening and narrowing on GBs. (a) Statistical data of the bandgap variation at the GBs with different tilt angles. The two blue triangles are results from Ref. [21]. (b) Structure of the model used in the DFT calculations. The GBs are modeled by the wrinkles with compressive strain along the armchair direction. (c) Total DOS of the pristine MoS_2 and the wrinkles with different strains (1%, 3%, 5%, and 7%). The blue and red arrows indicate the positions of the valence band and the conduction band, respectively.

mechanism has already been clarified, we focus on the physical origin of the bandgap broadening at the GBs. Our experiments reveal a long range and smooth nature of the bandgap variation (Fig. 3), indicating that the biaxial strain built up around the GBs has great impact on the electronic structures of the GBs. Considering such a strain-induced effect, we simply model the GBs by the bending of wrinkled structures along the z-direction in our DFT calculations. A compressive strain of 1% to 7% is applied to the lattice of the wrinkle along the armchair direction, as shown in Fig. 4(b). The DOS of the wrinkles is calculated after geometry relaxation, as illustrated in Fig. 4(c). The CBM is shifted away from the Fermi level as the strain is increased to 3% and is shifted towards the Fermi level as the strain is further increased to 5%. The VBM is only slightly shifted in the same direction of the CBM. These behaviors indicate that the strain can result in not only bandgap narrowing but also bandgap broadening, depending on the magnitude of the strain. For the wrinkle with a strain of 3%, the bandgap is broadened, and the CBM and VBM are shifted upward with respect to the intrinsic single-layer MoS_2. The upward band bending around the wrinkle can lead to significant charge transfer either between the flat

and rippled MoS_2 or between the MoS_2 and the substrate, which might contribute to the bandgap broadening at the GBs. We also model the GBs with a more realistic MoS_2 wrinkle structure consisting of a GB with a tilt angle of 16°. The results (Fig. S2(a) in the ESM) are similar to those of the simple model described in Fig. 4(c), confirming that a comprehensive strain is counted for the bandgap broadening of the GBs in single-layer MoS_2.

3 Conclusions

We studied the electronic structures of the GBs in single-layer MoS_2 on a HOPG substrate via LT-STM/STS. By measuring the dI/dV spectra of a series of GBs with tilt angles ranging from 0° to 25°, we found that the bandgaps at the GBs can be either broadened or narrowed with respect to the intrinsic single-layer MoS_2. DFT calculations reveal that the strain field around the GBs, as well as the charge-transfer effect, contributes to the bandgap broadening. Our work shows that the GBs can become more insulating, which may directly influence the transport properties of nanodevices based on polycrystalline single-layer MoS_2 and be useful for optoelectronics.

4 Methods

The growth of MoS_2 on graphite was as follows. Single-layer MoS_2 was grown on graphite using a three-temperature-zone CVD system. Prior to the growth of MoS_2, the HOPG was exfoliated to obtain a fresh surface. High-purity sulfur (Alfa Aesar 99.9%) and MoO_3 (Alfa Aesar 99.999%) powders were vaporized at 120 and 530 ℃, respectively, while the substrate was kept at 750 ℃. Ultrahigh-purity argon was used as the carrier with a flux of 130 sccm, and the growth time was 15 min.

The STM/STS experiments were conducted in an ultrahigh vacuum (base pressure of 1×10^{-10} mbar) LT-STM system (Unisoku). STM images were acquired in the constant-current mode. Differential conductance (dI/dV) spectra were collected by using a lock-in technique with 5-mV_{rms} sinusoidal modulation at a frequency of 973 Hz. All STM/STS experiments were performed with electrochemically etched tungsten tips at 4.3 K, which were calibrated with respect to the Au(111) surface state before and after spectroscopic measurements. The given voltages were referred to the sample.

DFT calculations were performed by using the Vienna *Ab initio* Simulation Package with the projected augmented wave. Wave functions were expanded in a plane-wave basis set to a 400-eV energy cutoff. The rippled MoS_2 was modeled by a (10 × 1) supercell (20 molybdenum atoms and 40 sulfur atoms) with the strain applied along the armchair direction, which consisted of a single-layer slab with a vacuum layer of 15 Å. All atoms were fully relaxed until the net force was smaller than 0.02 eV/Å. The MoS_2 structure under strain was simulated by fixing the length of the slab model. The bent MoS_2 structure with the lowest energy was obtained by optimizing the distance between the two outmost Mo atoms to release the strain in the out-of-plane direction. The Brillouin zone was sampled with a grid of (1 × 5 × 1).

Acknowledgements

We thank Sokrates T. Pantelides and Min Ouyang for their constructive suggestions. Financial support from the National Key Research & Development Projects (Nos. 2016YFA0300904 and 2016YFA0202300), the National Basics Research Program (Nos. 2013CB934500 and 2013CBA01600), and the National Natural Science Foundation of China (Nos. 51661135026, 61390501, 61390503, and 61325021) is gratefully acknowledged.

Electronic Supplementary Materials: Supplementary material (the method to determine the CBM and VBM; the bias-dependent STM images of the GB with a tilt angle of 20°; DFT calculations of the GBs with tilt angles of 16° and 25°; the apparent heights of the GBs relative to their neighboring flat MoS_2 regions) is available in the online version of this article at https://doi.org/10.1007/s12274-018-2128-3.

References

[1] Novoselov, K. S.; Geim, A. K.; Morozov, S. V.; Jiang, D.; Zhang, Y.; Dubonos, S. V.; Grigorieva, I. V.; Firsov, A. A. Electric field effect in atomically thin carbon films. *Science*

2004, *306*, 666–669.

[2] Mak, K. F.; Lee, C.; Hone, J.; Shan, J.; Heinz, T. F. Atomically thin MoS_2: A new direct-gap semiconductor. *Phys. Rev. Lett.* **2010**, *105*, 136805.

[3] Cheng, Y. C.; Yao, K. X.; Yang, Y.; Li, L.; Yao, Y. B.; Wang, Q. X.; Zhang, X. X.; Han, Y.; Schwingenschlögl, U. Van der Waals epitaxial growth of MoS_2 on SiO_2/Si by chemical vapor deposition. *RSC Adv.* **2013**, *3*, 17287–17293.

[4] Dumcenco, D.; Ovchinnikov, D.; Marinov, K.; Lazić, P.; Gibertini, M.; Marzari, N.; Sanchez, O. L.; Kung, Y. C.; Krasnozhon, D.; Chen, M. W. et al. Large-area epitaxial monolayer MoS_2. *ACS Nano* **2015**, *9*, 4611–4620.

[5] Fu, L.; Sun, Y. Y.; Wu, N.; Mendes, R. G.; Chen, L. F.; Xu, Z.; Zhang, T.; Rummeli, M. H.; Rellinghaus, B.; Pohl, D. et al. Direct growth of MoS_2/h-BN heterostructures via a sulfide-resistant alloy. *ACS Nano* **2016**, *10*, 2063–2070.

[6] Liu, X. L.; Balla, I.; Bergeron, H.; Campbell, G. P.; Bedzyk, M. J.; Hersam, M. C. Rotationally commensurate growth of MoS_2 on epitaxial graphene. *ACS Nano* **2016**, *10*, 1067–1075.

[7] Yu, H.; Yang, Z. Z.; Du, L. J.; Zhang, J.; Shi, J. N.; Chen, W.; Chen, P.; Liao, M. Z.; Zhao, J.; Meng, J. L. et al. Precisely aligned monolayer MoS_2 epitaxially grown on h-BN basal plane. *Small* **2017**, *13*, 1603005.

[8] Mak, K. F.; McGill, K. L.; Park, J.; McEuen, P. L. The valley Hall effect in MoS_2 transistors. *Science* **2014**, *344*, 1489–1492.

[9] Saito, Y.; Nakamura, Y.; Bahramy, M. S.; Kohama, Y.; Ye, J. T.; Kasahara, Y.; Nakagawa, Y.; Onga, M.; Tokunaga, M.; Nojima, T. et al. Superconductivity protected by spin-valley locking in ion-gated MoS_2. *Nat. Phys.* **2016**, *12*, 144–149.

[10] Radisavljevic, B.; Kis, A. Mobility engineering and a metal-insulator transition in monolayer MoS_2. *Nat. Mater.* **2013**, *12*, 815–820.

[11] Radisavljevic, B.; Radenovic, A.; Brivio, J.; Giacometti, V.; Kis, A. Single-layer MoS_2 transistors. *Nat. Nanotechnol.* **2011**, *6*, 147–150.

[12] Lopez-Sanchez, O.; Lembke, D.; Kayci, M.; Radenovic, A.; Kis, A. Ultrasensitive photodetectors based on monolayer MoS_2. *Nat. Nanotechnol.* **2013**, *8*, 497–501.

[13] Kibsgaard, J.; Chen, Z. B.; Reinecke, B. N.; Jaramillo, T. F. Engineering the surface structure of MoS_2 to preferentially expose active edge sites for electrocatalysis. *Nat. Mater.* **2012**, *11*, 963–969.

[14] Van der Zande, A. M.; Huang, P. Y.; Chenet, D. A.; Berkelbach, T. C.; You, Y. M.; Lee, G. H.; Heinz, T. F.; Reichman, D. R.; Muller, D. A.; Hone, J. C. Grains and grain boundaries in highly crystalline monolayer molybdenum disulphide. *Nat. Mater.* **2013**, *12*, 554–561.

[15] Zhou, W.; Zou, X. L.; Najmaei, S.; Liu, Z.; Shi, Y. M.; Kong, J.; Lou, J.; Ajayan, P. M.; Yakobson, B. I.; Idrobo, J. C. Intrinsic structural defects in monolayer molybdenum disulfide. *Nano Lett.* **2013**, *13*, 2615–2622.

[16] Park, S.; Kim, M. S.; Kim, H.; Lee, J.; Han, G. H.; Jung, J.; Kim, J. Spectroscopic visualization of grain boundaries of monolayer molybdenum disulfide by stacking bilayers. *ACS Nano* **2015**, *9*, 11042–11048.

[17] Sangwan, V. K.; Jariwala, D.; Kim, I. S.; Chen, K. S.; Marks, T. J.; Lauhon, L. J.; Hersam, M. C. Gate-tunable memristive phenomena mediated by grain boundaries in single-layer MoS_2. *Nat. Nanotechnol.* **2015**, *10*, 403–406.

[18] Enyashin, A. N.; Bar-Sadan, M.; Houben, L.; Seifert, G. Line defects in molybdenum disulfide layers. *J. Phys. Chem. C* **2013**, *117*, 10842–10848.

[19] Zou, X. L.; Liu, Y. Y.; Yakobson, B. I. Predicting dislocations and grain boundaries in two-dimensional metal-disulfides from the first principles. *Nano Lett.* **2013**, *13*, 253–258.

[20] Najmaei, S.; Amani, M.; Chin, M. L.; Liu, Z.; Birdwell, A. G.; O'Regan, T. P.; Ajayan, P. M.; Dubey, M.; Lou, J. Electrical transport properties of polycrystalline monolayer molybdenum disulfide. *ACS Nano* **2014**, *8*, 7930–7937.

[21] Huang, Y. L.; Chen, Y. F.; Zhang, W. J.; Quek, S. Y.; Chen, C. H.; Li, L. J.; Hsu, W. T.; Chang, W. H.; Zheng, Y. J.; Chen, W. et al. Bandgap tunability at single-layer molybdenum disulphide grain boundaries. *Nat. Commun.* **2015**, *6*, 6298.

[22] Jeong, H. Y.; Lee, S. Y.; Ly, T. H.; Han, G. H.; Kim, H.; Nam, H.; Jiong, Z.; Shin, B. G.; Yun, S. J.; Kim, J. et al. Visualizing point defects in transition-metal dichalcogenides using optical microscopy. *ACS Nano* **2016**, *10*, 770–777.

[23] Bao, W.; Borys, N. J.; Ko, C.; Suh, J.; Fan, W.; Thron, A.; Zhang, Y. J.; Buyanin, A.; Zhang, J.; Cabrini, S. et al. Visualizing nanoscale excitonic relaxation properties of disordered edges and grain boundaries in monolayer molybdenum disulfide. *Nat. Commun.* **2015**, *6*, 7993.

[24] Ly, T. H.; Perello, D. J.; Zhao, J.; Deng, Q. M.; Kim, H.; Han, G. H.; Chae, S. H.; Jeong, H. Y.; Lee, Y. H. Misorientation-angle-dependent electrical transport across molybdenum disulfide grain boundaries. *Nat. Commun.* **2016**, *7*, 10426.

[25] Najmaei, S.; Liu, Z.; Zhou, W.; Zou, X. L.; Shi, G.; Lei, S. D.; Yakobson, B. I.; Idrobo, J. C.; Ajayan, P. M.; Lou, J. Vapour phase growth and grain boundary structure of molybdenum disulphide atomic layers. *Nat. Mater.* **2013**, *12*, 754–759.

[26] Yazyev, O. V.; Louie, S. G. Topological defects in graphene: Dislocations and grain boundaries. *Phys. Rev. B* **2010**, *81*, 195420.

[27] Tison, Y.; Lagoute, J.; Repain, V.; Chacon, C.; Girard, Y.; Joucken, F.; Sporken, R.; Gargiulo, F.; Yazyev, O. V.; Rousset, S. Grain boundaries in graphene on SiC(000(1)) substrate. *Nano Lett.* **2014**, *14*, 6382–6386.

[28] Sachs, B.; Britnell, L.; Wehling, T. O.; Eckmann, A.; Jalil, R.; Belle, B. D.; Lichtenstein, A. I.; Katsnelson, M. I.; Novoselov, K. S. Doping mechanisms in graphene-MoS_2 hybrids. *Appl. Phys. Lett.* **2013**, *103*, 251607.

[29] Lu, C. I.; Butler, C. J.; Huang, J. K.; Hsing, C. R.; Yang, H. H.; Chu, Y. H.; Luo, C. H.; Sun, Y. C.; Hsu, S. H.; Yang, K. H. O. et al. Graphite edge controlled registration of monolayer MoS_2 crystal orientation. *Appl. Phys. Lett.* **2015**, *106*, 181904.

[30] Zhang, C. D.; Johnson, A.; Hsu, C. L.; Li, L. J.; Shih, C. K. Direct imaging of band profile in single layer MoS_2 on graphite: Quasiparticle energy gap, metallic edge states, and edge band bending. *Nano Lett.* **2014**, *14*, 2443–2447.

[31] Cheiwchanchamnangij, T.; Lambrecht, W. R. L. Quasiparticle band structure calculation of monolayer, bilayer, and bulk MoS_2. *Phys. Rev. B* **2012**, *85*, 205302.

[32] Lee, C.; Yan, H. G.; Brus, L. E.; Heinz, T. F.; Hone, J.; Ryu, S. Anomalous lattice vibrations of single- and few-layer MoS_2. *ACS Nano* **2010**, *4*, 2695–2700.

[33] Rutter, G. M.; Crain, J. N.; Guisinger, N. P.; Li, T.; First, P. N.; Stroscio, J. A. Scattering and interference in epitaxial graphene. *Science* **2007**, *317*, 219–222.

[34] Addou, R.; Colombo, L.; Wallace, R. M. Surface defects on natural MoS_2. *ACS Appl. Mater. Interfaces* **2015**, *7*, 11921–11929.

[35] Huang, Y. L.; Ding, Z. J.; Zhang, W. J.; Chang, Y. H.; Shi, Y. M.; Li, L. J.; Song, Z. B.; Zheng, Y. J.; Chi, D. Z.; Quek, S. Y. et al. Gap states at low-angle grain boundaries in monolayer tungsten diselenide. *Nano Lett.* **2016**, *16*, 3682–3688.

[36] Liu, L. W.; Xiao, W. D.; Wang, D. F.; Yang, K.; Tao, T.; Gao, H. J. Edge states of graphene wrinkles in single-layer graphene grown on Ni(111). *Appl. Phys. Lett.* **2016**, *109*, 143103.

[37] Ma, C. X.; Sun, H. F.; Zhao, Y. L.; Li, B.; Li, Q. X.; Zhao, A. D.; Wang, X. P.; Luo, Y.; Yang, J. L.; Wang, B. et al. Evidence of van hove singularities in ordered grain boundaries of graphene. *Phys. Rev. Lett.* **2014**, *112*, 226802.